Degradable and Nanosegregated Elastomers with Multiblock Sequences of Biobased Aromatic Mesogens and Biofunctional Aliphatic Oligocarbonates

Watanabe, Yuya; Kato, Riki; Fukushima, Kazuki; Kato, Takashi

DOI:
10.1021/acs.macromol.2c01747

Document Version
Publisher's PDF, also known as Version of record

Citation for published version (Harvard):
Watanabe, Y, Kato, R, Fukushima, K & Kato, T 2022, 'Degradable and Nanosegregated Elastomers with Multiblock Sequences of Biobased Aromatic Mesogens and Biofunctional Aliphatic Oligocarbonates', *Macromolecules*, vol. 55, no. 23, pp. 10285–10293. https://doi.org/10.1021/acs.macromol.2c01747

Macromolecules

pubs.acs.org/Macromolecules

Article

Degradable and Nanosegregated Elastomers with Multiblock Sequences of Biobased Aromatic Mesogens and Biofunctional Aliphatic Oligocarbonates

Yuya Watanabe, Riki Kato, Kazuki Fukushima,* and Takashi Kato*

Cite This: *Macromolecules* 2022, 55, 10285−10293

Read Online

ACCESS | Metrics & More | Article Recommendations | Supporting Information

ABSTRACT: We have developed multiblock aromatic/aliphatic condensation polymers, comprising side-chain biofunctionalized aliphatic oligocarbonates and biobased aromatic ester triad mesogens up to 17 wt %. Nanosegregation of the aromatic mesogen-rich domains with diameters of approximately 10 nm from the soft aliphatic polymer matrix is suggested by atomic force microscopy. The polymers exhibit rubberlike properties, unlike the corresponding aliphatic polycarbonate forming viscous liquid. These properties support the interchain interactions between the aromatic mesogens, which can serve as physical cross-linking. The aromatic ester triad mesogens in the multiblock polymers significantly bolster the tolerance to organocatalytic hydrolysis and methanolysis of the polymer chains but are eventually degraded. The multiblock polymers show degradation behavior slightly faster than poly(L-lactide), whereas poly(ethylene terephthalate) remains intact under the same condition. The present study demonstrates the efficacy of aromatic ester triad mesogens incorporated into the sequences of biodegradable aliphatic polycarbonates to enhance their physical properties while retaining degradability.

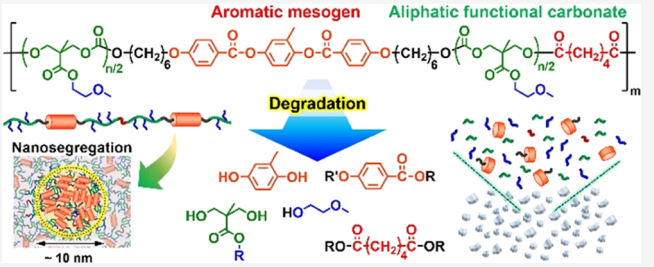

INTRODUCTION

Polymeric liquid crystals are widely utilized as functional materials, with applications ranging from high-strength engineering plastics to smart materials.[1−7] Main-chain aromatic liquid crystalline (LC) polyesters have been developed as high-strength plastics, owing to their advantages in processibility compared to aromatic polyamides and aromatic polyimides.[1,6,7] They can be processed by melt injection moldings, which orient the polymer main chain by exploiting the thermal LC properties. The alignment of rigid aromatic units in the main-chain LC polyesters leads to the formation of the ordered structure and the induction of anisotropy of physical properties, including electric and optical characteristics.[1,4−7]

Main-chain polymers such as aliphatic polycondensates, poly(L-lactide) (PLLA), and poly(trimethylene carbonate) (PTMC) have recently attracted considerable attention as synthetic biodegradable polymers.[8,9] They exhibit reasonable physical properties and are commercially available in fibers, fabrics, and films. However, their thermal and mechanical properties are limited compared with those of aromatic condensation polymers. Thus, combining aromatic and aliphatic sequences can be a possible synthesis strategy to achieve polymers with enhanced properties.[10] For instance, poly(butylene succinate-*co*-terephthalate) is designed to improve the biodegradability of poly(butylene terephthalate), an engineering thermoplastic, and to compensate for the physical properties of a biodegradable polyester, poly(butylene succinate).[10−12]

For aliphatic biodegradable condensation polymers, side-chain modification has often been employed to add bio-related functions such as water solubility (hydrophilicity), ionic properties, and stimuli responsiveness.[13−15] However, it remains challenging to form side-chain-functionalized aliphatic condensation polymers that meet biofunctions and physical stabilities.

In the present study, we have devised aromatic/aliphatic multiblock condensation polymers **P1a−c** comprising rigid rod aromatic mesogens and side-chain biofunctionalized aliphatic oligocarbonates (Figure 1). Polymers **P1a−c** are derived from mesogen-containing oligocarbonates **OC1a−c** through polycondensation with adipoyl chloride to form high-molecular-weight polymers. The aromatic ester triad mesogen structure in **P1a−c** and **OC1a−c** is well studied and expected to impart thermal stability to the polymers.[16−19] In addition, the mesogen is derived from 4-hydroxybenzoic acid and methylhydroquinone, which are currently recognized as

Received: August 22, 2022
Revised: October 22, 2022
Published: November 15, 2022

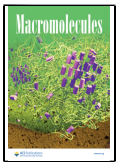

https://doi.org/10.1021/acs.macromol.2c01747
Macromolecules 2022, 55, 10285−10293

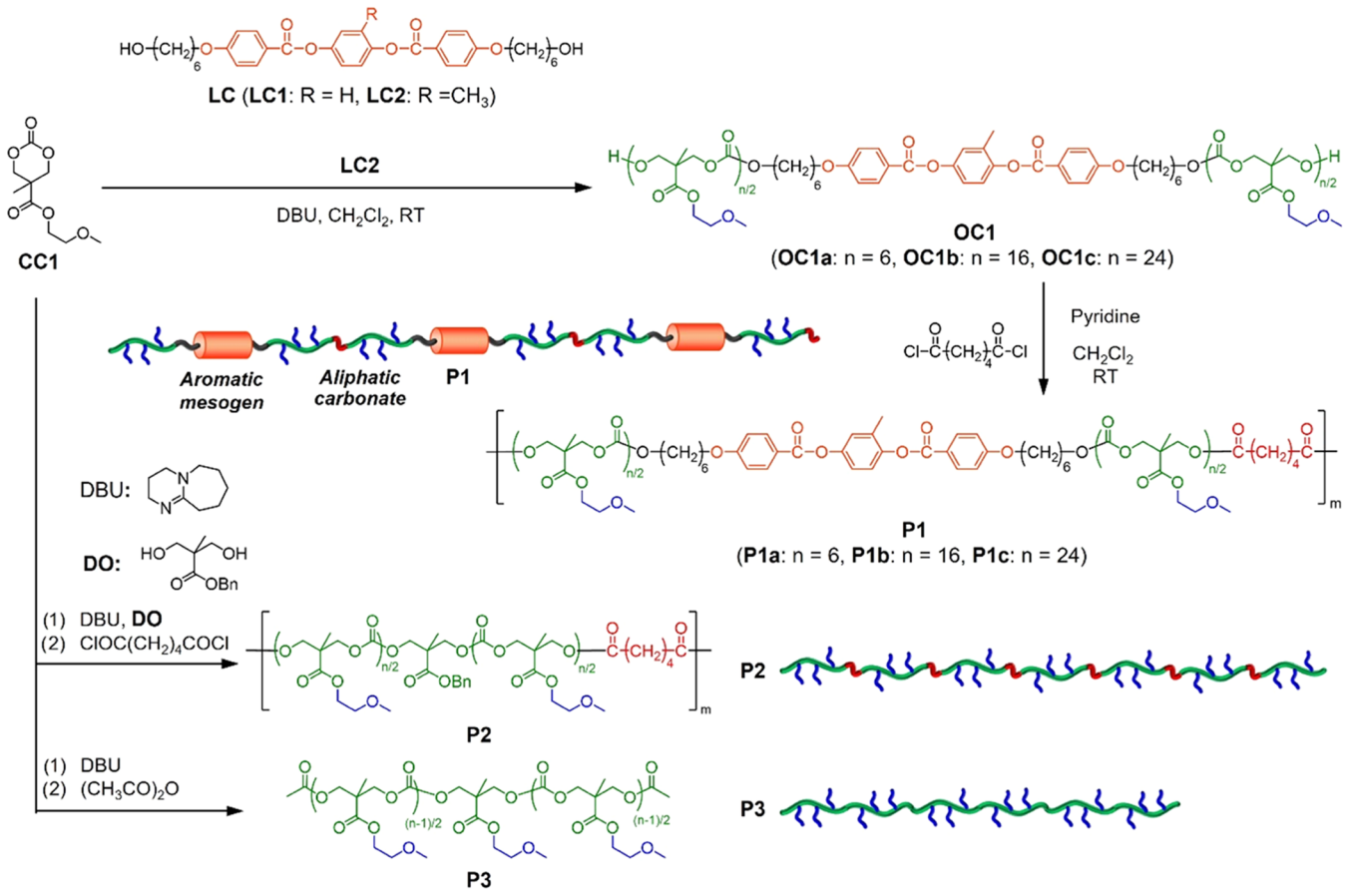

Figure 1. Synthesis of multiblock aromatic/aliphatic condensation polymers **P1a−c**.

potential biobased molecules.[20,21] Thus, this macromolecular design can be regarded to be benign to the environment and the biological system.

The aliphatic oligocarbonate segment with ether side chains **P3**, which is incorporated into **P1a−c** and **OC1a−c**, was previously reported as a biocompatible and biodegradable polymer.[22] **P3** is viscous and insoluble in water, showing a glass transition temperature (T_g) at around −20 °C.[22] These properties promise nonbiomedical applications such as adhesives and electrolytes.[23,24] Increasing T_g and mechanical properties will further expand the scope of applications for this polymer. Consequently, the synthetic strategy for **P1a−c** *via* aromatic mesogens and chain extension will be of great significance for improving the physical properties and increasing the molecular weights of **P3** (Figure 1). **P2** was also synthesized as a comparative example to evaluate the physical properties of **P1a−c**. Our macromolecular design is to incorporate the mesogenic structure into the main chain of the aliphatic condensation polymers. For other examples of the combination of biodegradable polymers and mesogenic structure, Hegmann et al. reported LC elastomers including a poly(ε-caprolactone) (PCL) derivative bearing a cholesterol moiety at the side chains, which exhibited LC properties and cell scaffold functions.[25,26]

Moreover, degradability of polymers is of interest to a broad range of materials scientists in the current circumstances requiring sustainable materials and circular economy including recycling and upcycling of materials.[27−30] Chemical recycling and depolymerization of polycarbonates are studied as well as polyesters.[28,29] Aliphatic polycarbonates are less susceptible to hydrolysis than aliphatic polyesters.[31,32] Thus, they can be applied to materials with durability of more than years and potential degradability and recyclability. Besides water, we can use short-chain alcohols and their derivatives derived from renewable resources[33,34] for chemical recycling of the polymers. Mecking and co-workers recently reported aliphatic polycarbonates and polyesters with longer alkylene main chains, which can be recycled by ethanolysis upon heating.[35] Herein, we have also investigated the degradability of the multiblock polymers in the inhomogeneous system using water and methanol as green degradation media. The present study sheds light on degradability of aromatic mesogens, which has not been well explored.

RESULTS AND DISCUSSION

Diol-Functionalized Mesogens. New diol-functionalized aromatic ester triad mesogens **LC1** and **LC2** (the chemical structure of which is already shown in the top part of Figure 1) were designed and synthesized to incorporate the aromatic unit into the polymer main chain (Supporting Information). Table 1 and Figures 2 and 3 present the molecular structures and LC properties of **LC1−4**. Aromatic ester triad mesogens with flexible end groups are known to be capable of showing thermally stable LC phases. The compounds containing the same triad mesogen with methoxy, butoxy, and hexyloxy groups as **LC1** and **LC2** showed the LC−isotropic transition at 252,[36] 206,[17] and 172 °C,[37] respectively. Interestingly, the LC phase was observed for **LC1** and **LC2** containing the hydroxy group capable of hydrogen bonding at the end of the hexamethylene chain. To examine the effects of the hydroxyl

https://doi.org/10.1021/acs.macromol.2c01747
Macromolecules 2022, 55, 10285−10293

Table 1. Thermal Properties of LC1−4

compound	phase transition behavior[a]				
LC1	Cr	146	N	188	I
LC2	Cr	103	N	169	I
LC3[b]	Cr	121	N	211	I
LC4[c]	Cr	89	N	172	I

[a]Cr, crystalline; N, nemtatic; I, isotropic. Phase transition temperatures (°C) were determined by DSC on the second heating process (5 °C min^{-1}, N_2). [b]Reported data from ref 38. [c]Reported data from ref 37.

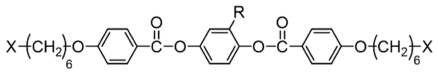

LC1: R = H, X = OH
LC2: R = CH_3, X = OH
LC3: R = H, X =H
LC4: R = CH_3, X = H

Figure 2. Structures of **LC1−4**.

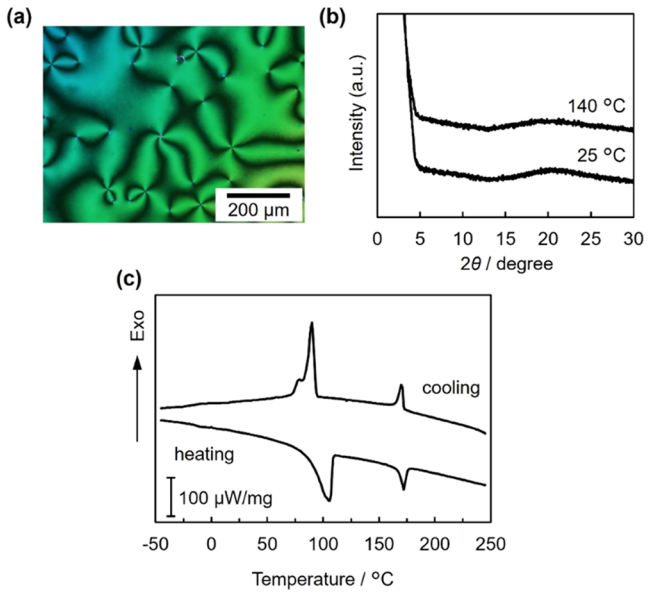

Figure 3. Liquid crystallinity of **LC2**. (a) Polarizing optical microscopy (POM) image at 120 °C. (b) XRD profiles at 25 and 140 °C cooled from the isotropic state at 170 °C. (c) DSC thermograms measured at a rate of 5 °C min^{-1}.

group and the lateral substituent on the mesogen on thermal properties and solubility, the LC behaviors of **LC1** and **LC2** were compared with those of **LC3** and **LC4** (Table 1). All compounds exhibit only nematic phases. The introduction of the lateral methyl group decreases melting and isotropization temperatures due to disturbing the close and stable packing of the aromatic mesogens. The highest (N → I) temperature is observed for **LC3**. The introduction of the lateral methyl substituent also induced lowering of the melting (Cr → N) temperatures. It is of interest that the induction of thermally stable nematic phases was observed for **LC1** and **LC3**.

Mesogen-Containing Oligocarbonates. Mesogen-containing oligocarbonates **OC1a−c** were synthesized through the ring-opening polymerization (ROP) of cyclic carbonate **CC1** using **LC2** as an initiator (Figure 1). **CC1** was prepared as previously reported.[22] The effects of the substituent on the solubility were observed for **LC1** and **LC2**. The methyl substituent in **LC2** offers higher solubility in various conventional organic solvents because of the asymmetric structure,[36,37] enabling the ROP of **CC1** in CH_2Cl_2, a preferable solvent for controlled polymerization by organic catalysts such as 1,8-diazabicyclo[5.4.0]undec-7-ene (DBU).[39,40] **LC1** showed very poor solubility in CH_2Cl_2. The **LC2**-initiated ROP of **CC1** successfully proceeded in a controlled manner. Size exclusion chromatography (SEC) traces of **OC1a−c** were monomodal (Figure 4a), and the molecular-weight dispersities ($Đ_M = M_w/M_n$; Table S1) were below 1.2. In addition, the high end-group fidelity of **OC1a** was confirmed by ^{1}H NMR (the integral ratio of b'/h/m = 4/4/4 in Figure S1a) and matrix-assisted laser desorption ionization time-of-flight (MALDI-TOF) mass spectrometry (Figure 4b). The degrees of polymerization of the aliphatic oligocarbonate units (n) and the aromatic contents (W_{ar}) in **OC1a−c** were almost controlled by the ratio of **CC1** to **LC2**, affording various lengths of **OC1a−c** (Table S1).

Mesogen-Containing Multiblock Polymers. **OC1a−c** were then used as macrodiols[41] for polycondensation with adipoyl chloride to form multiblock condensation polymers **P1a−c** (Figure 1). It is practically challenging to feed equimolar amounts of acid dichlorides to the macrodiols with molecular-weight dispersity. Additional portions of the macrodiols and adipoyl chloride were loaded to obtain high-molecular-weight polymers (Figure S1b) in this polycondensation when either OH or Cl was confirmed to remain unreacted on ^{1}H NMR. The lower number of the repeating unit of the polycondensate (m in Table 2) with longer oligocarbonate segments resulted from a low frequency of the condensation reaction. As indicated in the SEC traces of **P1a−c** (Figure 4a), a significant shift and broadening of the elution peaks reflect the successful progress of the typical polycondensation reaction. High-molecular-weight polymers with weight-average molecular weights (M_w) of more than 100 × 10^3 were obtained.

The mesogen-containing multiblock polymers **P1a−c** exhibited an elastic and rubberlike form (Figure 5a), while the ether-functionalized aliphatic polycarbonate **P3** formed a viscous liquid state (Figure 5b). These results suggest that the mechanical properties of **P1a−c** can be attributable to the multiblock structure achieved by conjugating aromatic ester triad mesogens in the main chain and increasing the molecular weight to up to 148 × 10^3.

Surface Nanostructure: Nanosegregation. We envisioned that molecular assemblies of the aromatic mesogens in the multiblock polymers serve as physical cross-linking nanodomains, as often realized in LC elastomers.[3,25,42,43] Hence, we employed atomic force microscopy (AFM) to observe the nanostructures on the surfaces of **P1a−c** and **P2** (Figure 6). The AFM samples were obtained by spin-coating $CHCl_3$ solutions of **P1a−c** and **P2** on silicon wafers and drying in air and vacuum at room temperature for 2 days. The height image of **P1a** obtained by the conventional tapping mode showed a smooth surface with small dark dots, consistent with bright spherical domains with diameters of approximately 10 nm in the phase image (Figure 6a). These images suggest the presence of phase-segregated nanostructures[43] in **P1a**. The fraction of the bright nanodomains increased over time and was saturated over several days (Figure S2b). The area fraction of the bright nanodomains in the phase images was relevant to the aromatic contents in the polymers; fewer bright dots were observed in the phase images of **P1b** and **P1c** than in those of

https://doi.org/10.1021/acs.macromol.2c01747
Macromolecules 2022, 55, 10285−10293

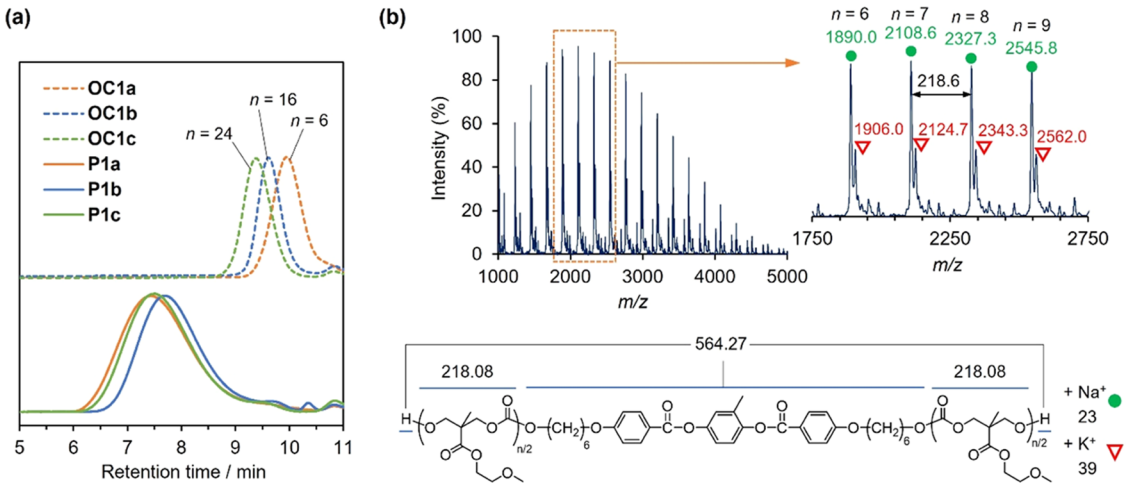

Figure 4. Molecular weight analyses of **OC1a–c** and **P1a–c**. (a) SEC traces of **OC1a–c** and **P1a–c** measured at 40 °C using THF as an eluent. Polystyrene (PS) standards were used for calibration. (b) MALDI-TOF mass spectrum of **OC1a**.

Table 2. Characterization of the Mesogen-Containing Multiblock Polymers P1a–c

	n^a	M_n ($\times 10^3$)^b	M_w ($\times 10^3$)^b	$Đ_M{}^b$	m^c	W_{Ar} (wt %)^d	T_g (°C)^e
P1a	6	48	148	3.1	18	17	−15
P1b	16	46	93	2.0	11	8	−18
P1c	24	44	135	3.1	9	6	−17
P2	8	34	66	2.0	14	0	−16
P3	125	18	24	1.4		0	−20

[a]Degree of polymerization of oligo-/polycarbonates determined by ^{1}H NMR. [b]Determined by SEC using PS standards (THF, 40 °C). [c]Number of repeating units of **P1** comprising **OC1** and adipate ester calculated based on M_n values determined by SEC. [d]Aromatic content of the polymer determined by ^{1}H NMR. [e]Glass transition temperature determined by DSC.

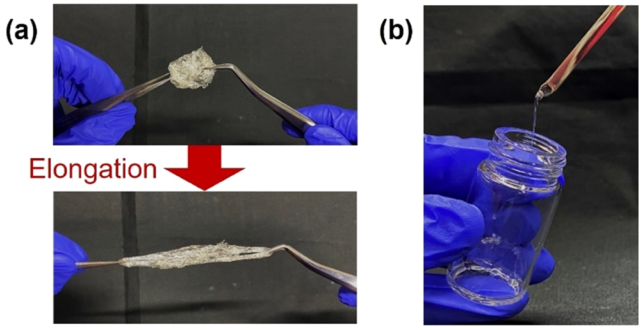

Figure 5. Physical appearances of mesogen-containing multiblock polymer **P1a** (a) and aliphatic polycarbonate **P3** (b).

P1a (Figure S2b,d,f). Similar to **P2** (Figure 6b), larger dark domains observed in the phase images of **P1b** and **P1c** (Figure S2d,f) were presumably because of the aliphatic oligocarbonate segments.

We then applied the PeakForce quantitative nanomechanical mapping (PF-QNM) mode,[45,46] which reads out modulus, adhesion, deformation, and energy dissipation, to visualize surface elasticity and softness and their distribution in **P1a–c**. Smooth surfaces were observed in the PF-QNM mode images of **P1a** using the same cantilever as the tapping mode (Figure S3a). The surface may be affected by scanning of the cantilever with a relatively high spring constant (k = 26 N m^{-1}). Thus, we conducted the PF-QNM mode observation using a cantilever with a lower spring constant (k = 0.7 N m^{-1}). A uniform modulus was observed in the modulus images, whereas small dark domains with diameters of approximately 10 nm were detected in the energy dissipation images (Figure 6c). The sizes and distribution of the dark domains appear to be consistent with the bright domains found in the phase image (Figure 6a, right). These results indicate that the bright small domains in the phase image are more elastic than those in the outer matrix part. Moreover, the height image in the PF-QNM mode also exhibited convex domains with diameters of approximately 10 nm and heights of up to 4 nm (Figure S3b). Consequently, these AFM studies revealed the presence of high-modulus domains induced by phase-segregated aromatic mesogens in **P1a–c**, possibly serving as physically cross-linked nanodomains, as illustrated in Figure 7a.

Estimation of Surface Elasticity. The PF-QNM mode imparts modulus information of the surface based on the Derjaguin–Müller–Toporov (DMT) model[47] (Supporting Information). The modulus is called the DMT or the reduced Young's modulus $E^* = E/(1 - \nu^2)$, where E is Young's modulus and ν is Poisson's ratio of the sample.[45,46] The spin-coated polymer samples were annealed at 150 °C for 10 min to obtain a uniform surface for the modulus measurement (Figure S4). The measurements were conducted at three different views per polymer. The modulus image in this study (Figures 6c and S4) comprised 512 × 512 pixels, each of which includes the DMT modulus. An averaged E^* value was calculated for each view and followed by averaging the values for the three different views, as shown in Figure 6d.

It should be noted that the reduced Young's moduli E^* were applied as the relative index of the surface modulus of the polymers with unknown Poisson's ratios. Ether-functionalized polycarbonate **P3** and its nonmesogen-containing polycondensate derivative **P2** showed moduli of 84 and 77 MPa, respectively (Figure 6d and Table S2). By contrast, **P1a–c** indicated the moduli of 2.3–3.6 × 10^2 MPa, approximately threefold of moduli obtained for **P2** and **P3**. The values increased proportionally with the aromatic mesogen contents (Figure 6d). Even if the Poisson's ratios of the polymers take the possible limits (ν = 0 for **P2** and **P3** and 0.5 for **P1a–c**), the differences in the calculated Young's moduli between **P1a–c** and **P2** or **P3** would be significant (Table S2). Accordingly,

https://doi.org/10.1021/acs.macromol.2c01747
Macromolecules 2022, 55, 10285–10293

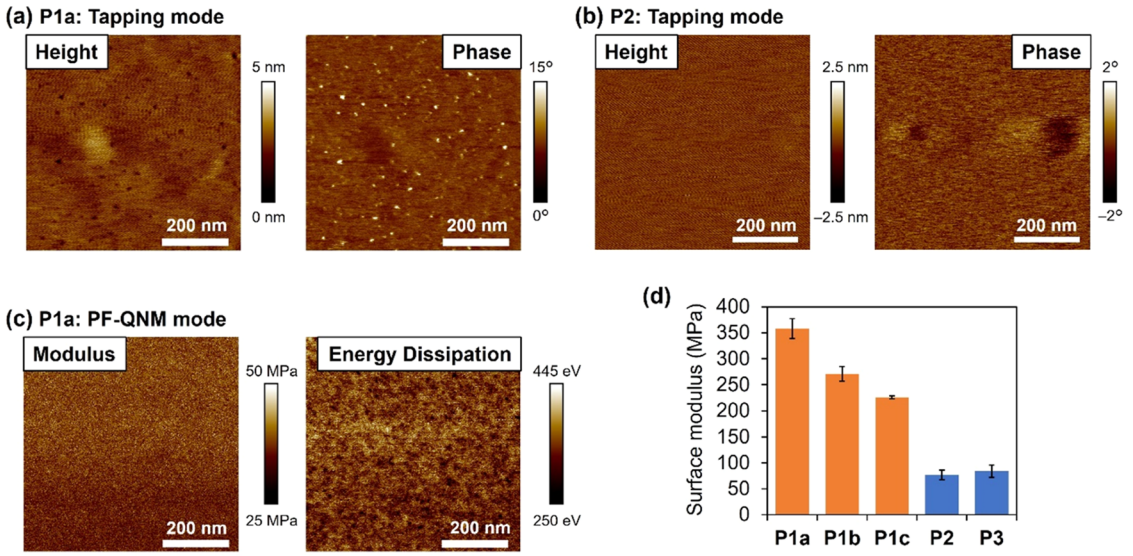

Figure 6. Nanostructure and nanomechanical studies of the polycondensates by atomic force microscopy. (a,b) Tapping mode images and (c) PF-QNM mode images of **P1a** and **P2**. The tapping mode observation was performed 2 days after spin coating using a cantilever with a spring constant k = 26 N m^{-1}. The PF-QNM mode observation was conducted 15 days after spin coating using a cantilever of k = 0.7 N m^{-1}. (d) Surface moduli of polymers obtained by the PF-QNM mode (mean ± SD, n = 3). The moduli were given as the reduced Young's moduli based on the DMT model.

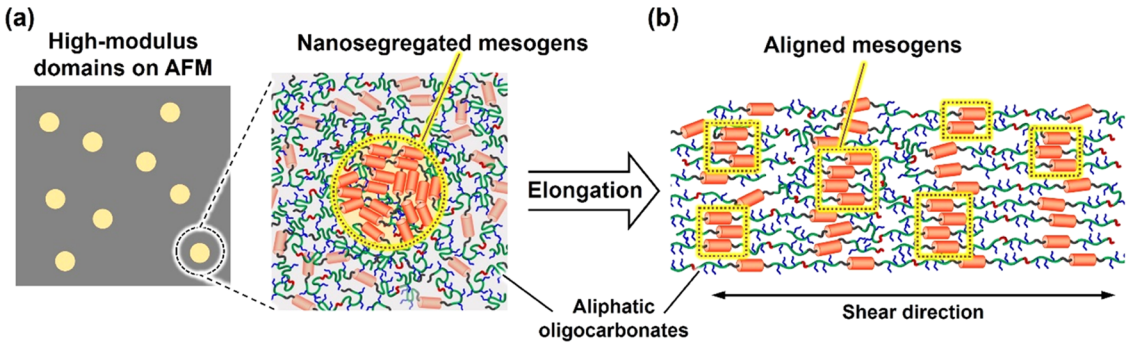

Figure 7. Schematic representations of nanostructures of mesogen-containing multiblock polymers **P1a−c** driven by nanosegregation of mesogens reflecting AFM images (a) and aligned by shear stress (b).

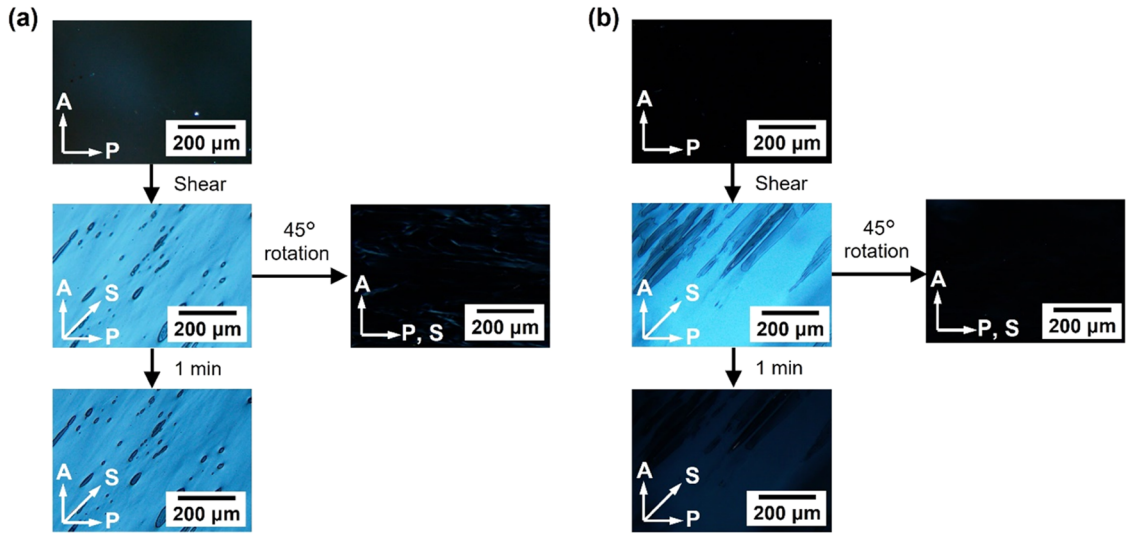

Figure 8. POM images of **P1a** (a) and **P2** (b). The polymers were sheared at room temperature and left for 1 min. Arrows are directions of the analyzer (A), shear (S), and polarizer (P).

this AFM technique could quantitatively evaluate the great enhancement of the elasticity in **P1a−c**.

The elastic moduli of the polymer surface calculated by the PF-QNM mode of AFM are often inconsistent with those

https://doi.org/10.1021/acs.macromol.2c01747
Macromolecules 2022, 55, 10285−10293

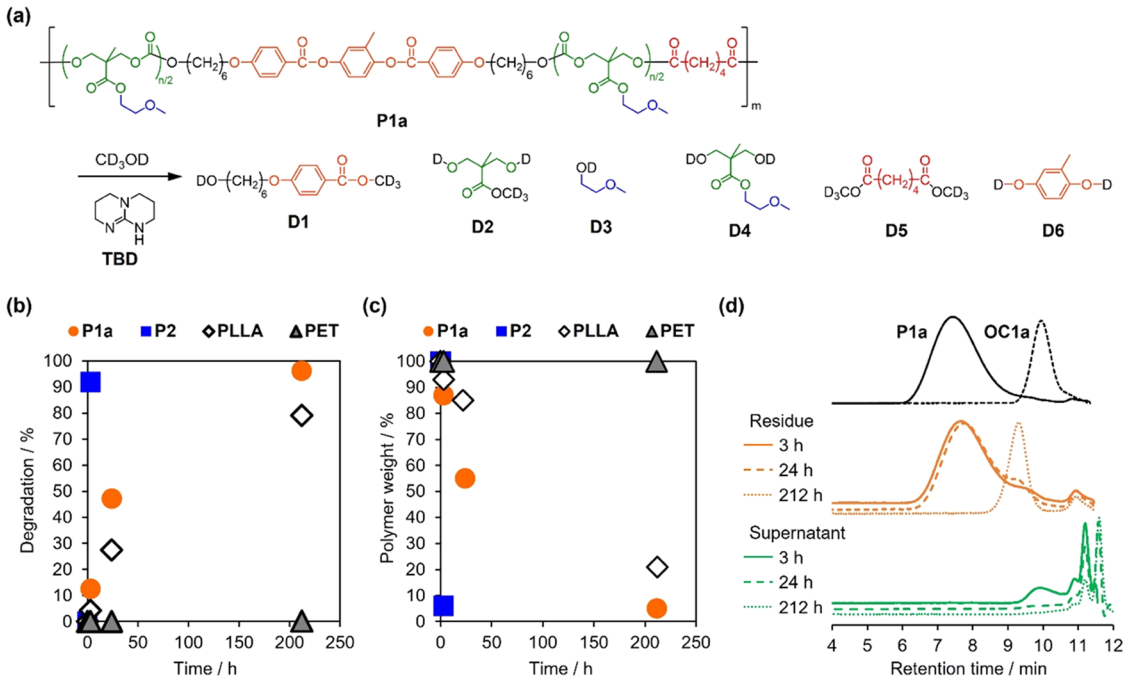

Figure 9. Degradation behavior of polymers in methanol with TBD. (a) Structures of possible degradates generated by methanolysis of **P1a**. (b) Extent of degradation and (c) weight fractions of polymer residues in CD_3OD as a function of time. (d) SEC traces (THF, 40 °C) of the supernatant and residue parts of **P1a** subjected to methanolysis.

obtained by a conventional stress−strain test of the bulk sample, as reported by Sokolov.[46] We measured the surface moduli of PTMC and PCL as representative aliphatic polycarbonate and polyester using the PF-QNM mode. Their calculated Young's moduli using the reported Poisson's ratios were 46 and 1.6 × 10^3 MPa for PTMC and PCL, respectively (Table S2). The respective values of PTMC and PCL at the bulk state are reported to be 3−7 and 2.1−4.4 × 10^2 MPa.[48,49] The actual Young's moduli of mesogen-containing multiblock copolymers **P1a−c** at the bulk state were speculated to be lower than those calculated in this study (Table S2). Nonetheless, this nanomechanical evaluation is undoubtedly practical for discussing the relative elasticity under the same conditions. These results demonstrated that **P1a−c** became more elastic than PTMC and softer than PCL.

Influences of Aromatic Mesogens on Self-Assembly Behavior of Multiblock Polymers. The XRD profiles of **P1a−c** exhibited no peaks, similar to those of nonmesogen-containing polymers **P2** and **P3** (Figure S5). The POM images of **P1a−c** indicate that none of the polymers inserted between the polyimide-coated glass slides showed birefringence, regardless of the aromatic contents (Figure S6). These results suggest that **P1a−c** do not form ordered structures. When **P1a−c** inserted between the glasses were sheared, they showed bright-polarized images, which are considered to be induced by the aligned molecules (Figures 8a and S6). Similarly, the polarized image of **P2** appeared bright as a response to shear (Figure 8b). The brightness reduced shortly for **P2** while maintained at 1 min after shearing for **P1a** (Figure 8). This delayed fading is attributed to the presence of nanosegregated mesogens,[44] serving for fixing the aligned molecules by shear (Figure 7b). The fading rate was associated with the aromatic contents in **P1a−c** (W_{ar} in Table 1), as the POM images darkened at 1 min after shearing for **P1b** and **P1c** with lower aromatic contents than **P1a** (Figure S6). These POM studies suggest that the aromatic rigid rod mesogens are capable of maintaining the alignment of polymer chains induced by shear stress (Figure 7b). Furthermore, the aromatic mesogens regularly arrayed by the aliphatic oligocarbonates of controlled length may be responsible for the delayed fading of the bright-polarized images (Figure 8a).

Degradation Study of Polymers. Degradation of polymers **P1a** and **P2** in liquid media was investigated by ^{1}H NMR using deuterated methanol (CD_3OD) and water (D_2O), as previously reported.[50] Since **P3** is known to be stable in methanol and water without catalysts and enzymes,[22] we used 1,5,7-triazabicyclo[4.4.0]dec-5-ene (TBD) as an organic catalyst to actively induce the degradation as performed in chemical recycling and upcycling of aromatic polyesters and polycarbonates.[51,52] PLLA and poly(ethylene terephthalate) (PET) were used as controls.

Bulk polymers were placed in the deuterated solvents containing 10 wt % TBD relative to the polymers, which were stirred for the predetermined time at room temperature and 40 °C for CD_3OD and D_2O solutions, respectively. No polymers were soluble in CD_3OD and D_2O initially. All polymers were degraded by TBD-catalyzed methanolysis, as supported by emerging signals in ^{1}H NMR spectra of the supernatants (Figures S7−S10) and the disappearance of samples in CD_3OD, except for PET. The degradation products (degradates) of **P1a** and **P2** were identified to include **D1−D6** and **D2−D5** (Figure 9a), respectively, according to the relevant ^{1}H NMR data of the intermediates (Figures S7 and S8). The signals observed in the supernatants of degradation media for PLLA and PET matched methyl lactate and a trace amount of dimethyl terephthalate, respectively (Figures S9 and S10). The extent of degradation was quantified based on integral ratios of the degradates and TBD (Figure 9b). The residues in CD_3OD were thoroughly dried in vacuum and weighed. The time courses of the weight changes of the

https://doi.org/10.1021/acs.macromol.2c01747
Macromolecules 2022, 55, 10285−10293

residues in CD_3OD are plotted in Figure 9c. The formation of soluble degradates and the weight change of the insoluble residues in CD_3OD were almost complementary (Figure 9b,c), suggesting the validity of quantification using NMR.

The methanolytic degradation of **P2** was mostly completed in 3 h, as the residual weight fraction was less than 10% (Figure 9c). **P1a** showed slower degradation than **P2** (Figure 9b,c), indicating the contribution of 17 wt % aromatic mesogen to the resistance to methanolysis. Nevertheless, ^{1}H NMR spectra of the supernatant of **P1a** revealed that the degradation of the aromatic mesogen structure occurred from the beginning of methanolysis (Figure S7, t = 3 h). This can be reasonable because the carbonyl group of aryl benzoate (a building block of mesogen) is more electrophilic than that of alkyl benzoate (a building block of PET). The methanolysis of PLLA proceeded slightly slower than that of **P1a** (Figure 9b,c). The NMR study revealed that PET was also slightly degraded by the TBD-catalyzed methanolysis at room temperature (∼0.2%).

The shapes and retention times of SEC traces of degradation residues of **P1a** and **P2** did not change until 24 h, indicating that this inhomogeneous degradation proceeds with the surface erosion mechanism as with other common aliphatic polycarbonates (Figures 9d and S11a).[14] The residue of **P1a** at 212 h comprised lower-molecular-weight fractions, which appeared close to **OC1a** (Figure 9d, orange). The supernatant of degradation media of **P1a** at 3 h included further lower-molecular-weight fractions, whose intensity gradually decreased afterward (Figure 9d, green). By contrast, PLLA was subjected to bulk erosion, and thus, the residue at 24 h already showed bimodal SEC traces due to the concomitant formation of low-molecular-weight fractions (Figure S11b).

The affinity of polymers to methanol, including swelling, should be considered to explain the susceptibility of polymers to methanolysis. PLLA used in this study contains crystalline parts predominantly (Figure S12), which impede the infiltration of methanol. In a similar manner, nanosegregated structures and nanodomains formed by the aromatic mesogens may enhance the tolerance to TBD-catalyzed methanolysis of **P1a**.

For the organocatalytic hydrolysis, all polymers remained in D_2O after 1 week, and the weight changes were negligible. In the ^{1}H NMR spectra of the supernatant of the D_2O solutions, **P1a**, **P2**, and PLLA indicated small and distinct signals characteristic of the monomer unit structures, whereas PET did not show any water-soluble fractions (Figures S13−S16). The levels of degradation were estimated from the integral ratios of TBD and the soluble structures stemming from the polymers, which were 0.3, 0.9, and 1.0% for **P1a**, **P2**, and PLLA, respectively. These results indicate that **P1a** is stable in water and that the aromatic mesogen serves to enhance the tolerance to hydrolysis. Consequently, **P1a** is stable in an aqueous environment but is readily degraded and recycled by catalytic methanolysis at room temperature. These media-dependent degradation properties of **P1a** may contribute to developing sustainable soft materials and elastomer and their low-energy and low-carbon-emission recycling process.

Thermal Properties of Polymers. The aromatic ester triad mesogens did not significantly influence the thermal properties of **P1a−c**. Unlike **LC1** and **LC2**, no phase transition was observed above T_g on the DSC thermograms of **P1a−c** and **OC1a−c**, suggesting that these materials contain no recognizable LC and crystalline phases (Figures S17 and S18). There are slight differences in T_g between **P1a−c**, **P2**, and **P3**, which appear to be associated with their M_w (Table 2 and Figures S17 and S18). These results show that the molecular interactions between the aromatic mesogens in **P1a−c** are dynamic and induce the nanosegregated structures (Figure 7a). The multiblock structure of **P1a−c** is unique and different from those of main-chain LC polymers and their block copolymers.[53]

The glass transitions of **P1a−c** appeared at higher temperatures than those of corresponding oligocarbonates **OC1a−c** (Figures S17 and S18) due to the increase in the molecular weights of **P1a−c**. Similar to **P3**, **OC1b** and **OC1c** exhibited the glass transitions in the vicinity of −20 °C, while that of **OC1a** appeared at around −30 °C (Figure S18). No birefringence was observed in the POM images of **OC1a−c** (Figure S19), indicating that distinct ordered phases were not formed in **OC1a−c**. These results show that the aromatic mesogens incorporated up to 17 wt % do not significantly influence the thermal properties of aliphatic oligocarbonates. In other words, for **OC1a** with the shortest oligocarbonate units, six units of aliphatic carbonates bearing ether side chains were found to sufficiently interrupt the formation of the LC phase by the aromatic mesogens.

The thermal decomposition properties of **P1a−c** and **OC1a−c** were related to the aromatic mesogen contents, although there was no significant difference in the 5% weight loss temperature (Figure S20). Aliphatic oligocarbonate segments were decomposed initially, followed by the decomposition of the other parts. The slopes of the thermogravimetry weight loss curves appear to depend on the aromatic contents of **P1a−c** and **OC1a−c**. However, their decomposition behavior does not directly reflect their aromatic/aliphatic compositions. The weight loss of **OC1a**, containing more than 80 wt % of aliphatic carbonates, was alleviated at around 40% of weight loss (Figure S20b). The molecular interactions of the aligned mesogens may retard the thermal degradation of the aliphatic part.

CONCLUSIONS

Nanosegregated multiblock aromatic/aliphatic condensation polymers bearing ether side chains were successfully synthesized to enhance their mechanical and thermal properties. Moreover, the controllability of degradation of aliphatic condensation polymers as additional functionality was achieved by the incorporation of aromatic mesogens into the main chains. The polymers exhibited elastic properties in bulk due to the dynamic nanosegregation of weakly interacted aromatic mesogens. The repeating sequences consisting of the aromatic ester triad mesogen and aliphatic oligocarbonates with the controlled length may be responsible for these notable thermal and mechanical properties. These weak and dynamic interactions may be beneficial for applications in soft tissue regeneration as well as sustainable soft material. The degradation study revealed that multiblock polymers were stable in water but degraded in methanol at room temperature, affording degradation of the aromatic mesogen. The present study suggests that the aromatic ester triad structure is beneficial for enhancing physical properties of aliphatic condensation polymers without loss of recyclability and sustainability.

https://doi.org/10.1021/acs.macromol.2c01747
Macromolecules 2022, 55, 10285−10293

■ ASSOCIATED CONTENT

Supporting Information

The Supporting Information is available free of charge at https://pubs.acs.org/doi/10.1021/acs.macromol.2c01747.

Experimental details, NMR spectra, AFM images, XRD profiles, POM images, DSC thermograms, and TG profiles (PDF)

■ AUTHOR INFORMATION

Corresponding Authors

Kazuki Fukushima − *Department of Chemistry and Biotechnology, School of Engineering, The University of Tokyo, Tokyo 113-8656, Japan; Japan Science and Technology Agency (JST), PRESTO, Kawaguchi, Saitama 332-0012, Japan;* orcid.org/0000-0002-6980-9663; Email: k_fukushima@chembio.t.u-tokyo.ac.jp

Takashi Kato − *Department of Chemistry and Biotechnology, School of Engineering, The University of Tokyo, Tokyo 113-8656, Japan; Research Initiative for Supra-Materials, Shinshu University, Wakasato, Nagano 380-8553, Japan;* orcid.org/0000-0002-0571-0883; Email: kato@chiral.t.u-tokyo.ac.jp

Authors

Yuya Watanabe − *Department of Chemistry and Biotechnology, School of Engineering, The University of Tokyo, Tokyo 113-8656, Japan;* orcid.org/0000-0001-8250-3258

Riki Kato − *Department of Chemistry and Biotechnology, School of Engineering, The University of Tokyo, Tokyo 113-8656, Japan;* orcid.org/0000-0001-6706-3151

Complete contact information is available at: https://pubs.acs.org/10.1021/acs.macromol.2c01747

Author Contributions

The manuscript was written through the contribution of all authors. All authors have given approval to the final version of the manuscript.

Notes

The authors declare no competing financial interest.

■ ACKNOWLEDGMENTS

This study was supported by JSPS KAKENHI grants (JP19H05714, JP19H05715, and JP19H05716), JST PRESTO grant (JPMJPR21N7), JST SPRING grant (JPMJSP2108), and Eno Science Foundation. Dr. Junya Uchida of The University of Tokyo is thanked for the valuable discussion and technical support on XRD and POM analyses. The authors are grateful to Dr. Yoshihisa Fujii of Mie University for helpful advice and discussion on AFM studies. The authors thank Editage (www.editage.com) for English language editing.

■ ABBREVIATIONS USED

LC, liquid crystalline; PLLA, poly(L-lactide); PTMC, poly(trimethylene carbonate); PCL, poly(ε-caprolactone); OC, oligocarbonate; POM, polarizing optical microscopy; XRD, X-ray diffraction; DSC, differential scanning calorimetry; ROP, ring-opening polymerization; CC, cyclic carbonate; DBU, 1,8-diazabicyclo[5.4.0]-7-undecene; SEC, size exclusion chromatography; NMR, nuclear magnetic resonance; MALDI-TOF, matrix-assisted laser desorption ionization time-of-flight; THF, tetrahydrofuran; PS, polystyrene; AFM, atomic force microscopy; PF-QNM, PeakForce quantitative nanomechanical mapping; DMT model, Derjaguin−Müller−Toporov model; TBD, 1,5,7-triazabicyclo[4.4.0]dec-5-ene; PET, poly(ethylene terephthalate); TG, thermogravimetry

■ REFERENCES

(1) Greiner, A.; Schmidt, H-W. Aromatic Main-Chain Liquid-Crystalline Polymers. In *Handbook of Liquid Crystals*, Goodby, J.; Collings, P. J.; Kato, T.; Tschierske, C.; Gleeson, H.; Raynes, P., Eds.; Wiley-VCH, 2014; pp 303−329.

(2) Uchida, J.; Soberats, B.; Gupta, M.; Kato, T. Advanced Functional Liquid Crystals. *Adv. Mater.* **2022**, *34*, No. 2109063.

(3) de Haan, L. T.; Verjans, J. M. N.; Broer, D. J.; Bastiaansen, C. W. M.; Schenning, A. P. H. J. Humidity-Responsive Liquid Crystalline Polymer Actuators with an Asymmetry in the Molecular Trigger That Bend, Fold, and Curl. *J. Am. Chem. Soc.* **2014**, *136*, 10585−10588.

(4) Ji, Y.; Bai, Y.; Liu, X.; Jia, K. Progress of Liquid Crystal Polyester (LCP) for 5G Application. *Adv. Ind. Eng. Polym. Res.* **2020**, *3*, 160−174.

(5) Lyu, X.; Xiao, A.; Shi, D.; Li, Y.; Shen, Z.; Chen, E-Q.; Zheng, S.; Fan, X.-H.; Zhou, Q-F. Liquid Crystalline Polymers: Discovery, Development, and the Future. *Polymer* **2020**, *202*, No. 122740.

(6) Kato, T.; Uchida, J.; Ichikawa, T.; Soberats, B. Functional Liquid-Crystalline Polymers and Supramolecular Liquid Crystals. *Polym. J.* **2018**, *50*, 149−166.

(7) Ober, C. K.; Jin, J-I.; Zhou, Q.; Lenz, R. W. Liquid Crystal Polymers with Flexible Spacers in the Main Chain. In *Liquid Crystal Polymers I.; Advances in Polymer Science*, Flory, P. J.; Uematsu, I.; Uematsu, Y.; Papkov, S. P.; Ober, C. H.; Jin, J-I.; Lentz, R. W., Eds.; Springer: 1984; Vol. *59*, pp 103−146.

(8) Fukushima, K.; Kimura, Y. Stereocomplexed Polylactides (Neo-PLA) as High-Performance Bio-Based Polymers: their Formation, Properties, and Application. *Polym. Int.* **2006**, *55*, 626−642.

(9) Zhu, K. J.; Hendren, R. W.; Jensen, K.; Pitt, C. G. Synthesis, Properties, and Biodegradation of Poly(1,3-trimethylene carbonate). *Macromolecules* **1991**, *24*, 1736−1740.

(10) Goodby, J. W. Liquid-Crystalline Polymers for Biomechanical Applications. In *Handbook of Liquid Crystals*, Goodby, J.; Collings, P. J.; Kato, T.; Tschierske, C.; Gleeson, H.; Raynes, P., Eds.; Wiley-VCH, 2014; pp 879−908.

(11) Witt, U.; Yamamoto, M.; Seeliger, U.; Müller, R. J.; Warzelhan, V. Biodegradable Polymeric Materials−Not the Origin but the Chemical Structure Determines Biodegradability. *Angew. Chem. Int. Ed.* **1999**, *38*, 1438−1442.

(12) Honda, N.; Taniguchi, I.; Miyamoto, M.; Kimura, Y. Reaction Mechanism of Enzymatic Degradation of Poly(butylene succinate-*co*-terephthalate) (PBST) with a Lipase Originated from *Pseudomonas cepacia*. *Macromol. Biosci.* **2003**, *3*, 189−197.

(13) Yu, W.; Maynard, E.; Chiaradia, V.; Arno, M. C.; Dove, A. P. Aliphatic Polycarbonates from Cyclic Carbonate Monomers and Their Application as Biomaterials. *Chem. Rev.* **2021**, *121*, 10865−10907.

(14) Fukushima, K. Poly(trimethylene carbonate)-Based Polymers Engineered for Biodegradable Functional Biomaterials. *Biomater. Sci.* **2016**, *4*, 9−24.

(15) Vaca, B. M.; Bourissou, M. *O*-Carboxyanhydrides: Useful Tools for the Preparation of Well-Defined Functionalized Polyesters. *ACS Macro Lett.* **2015**, *4*, 792−798.

(16) Ober, C.; Jin, J-I.; Lenz, R. W. Liquid Crystal Polymers.V. Thermotropic Polyesters with Either Dyad or Triad Aromatic Ester Mesogenic Units and Flexible Polymethylene Spacers in the Main Chain. *Polym. J.* **1982**, *14*, 9−17.

(17) Lenz, R. W. Synthesis and Properties of Thermotropic Liquid Crystal Polymers with Main Chain Mesogenic Units. *Polym. J.* **1985**, *17*, 105−115.

(18) Uryu, T.; Kato, T. Solid-State Cross Polarization/Magic Angle Spinning ^{13}C NMR Study of Thermotropic Aromatic Polyester

Containing a Flexible Spacer in the Main Chain. *Macromolecules* **1988**, *21*, 378−384.
(19) Kato, T.; Karbir, G. M. A.; Uryu, T. Solid-State CP/MAS ^{13}C-NMR Studies of Naphthalene-Based Thermotropic Polyesters and Model Compounds. *J. Polym. Sci., Part A: Polym. Chem.* **1989**, *27*, 1447−1465.
(20) Tomizawa, S.; Chuah, J.-A.; Matsumoto, K.; Doi, Y.; Numata, K. Understanding the Limitations in the Biosynthesis of Polyhydroxyalkanoate (PHA) from Lignin Derivatives. *ACS Sustainable Chem. Eng.* **2014**, *2*, 1106−1113.
(21) García-Caballero, M.; Marí-Beffa, M.; Cañedo, L.; Medina, M. Á.; Quesada, A. R. Toluquinol, a Marine Fungus Metabolite, is a New Angiosuppresor That Interferes the Akt Pathway. *Biochem. Pharmacol.* **2013**, *85*, 1727−1740.
(22) Fukushima, K.; Inoue, Y.; Haga, Y.; Ota, T.; Honda, K.; Sato, C.; Tanaka, M. Monoether-Tagged Biodegradable Polycarbonate Preventing Platelet Adhesion and Demonstrating Vascular Cell Adhesion: A Promising Material for Resorbable Vascular Grafts and Stents. *Biomacromolecules* **2017**, *18*, 3834−3843.
(23) Beharaj, A.; McCaslin, E. Z.; Blessing, W. A.; Grinstaff, M. W. Sustainable Polycarbonate Adhesives for Dry and Aqueous Conditions with Thermoresponsive Properties. *Nat. Commun.* **2019**, *10*, 5478.
(24) Tominaga, Y. Ion-Conductive Polymer Electrolytes Based on Poly(ethylene carbonate) and Its Derivatives. *Polym. J.* **2017**, *49*, 291−299.
(25) Gao, Y.; Mori, T.; Manning, S.; Zhao, Y.; Nielsen, Ad.; Neshat, A.; Sharma, A.; Mahnen, C. J.; Everson, H. R.; Crotty, S.; Clements, R. J.; Malcuit, C.; Hegmann, E. Biocompatible 3D Liquid Crystal Elastomer Cell Scaffolds and Foams with Primary and Secondary Porous Architecture. *ACS Macro Lett.* **2016**, *5*, 4−9.
(26) Prévôt, M. E.; Andro, H.; Alexander, S. L. M.; Ustunel, S.; Zhu, C.; Nikolov, Z.; Rafferty, S. T.; Brannum, M. T.; Kinsel, B.; Korley, L. T. J.; Freeman, E. J.; McDonough, J. A.; Clements, R. J.; Hegmann, E. Liquid Crystal Elastomer Foams with Elastic Properties Specifically Engineered as Biodegradable Brain Tissue Scaffolds. *Soft Matter* **2018**, *14*, 354−360.
(27) Hillmyer, M. A. The Promise of Plastics from Plants. *Science* **2017**, *358*, 868−870.
(28) Jehanno, C.; Alty, J. W.; Roosen, M.; De Meester, S.; Dove, A. P.; Chen, E. Y.-X.; Leibfarth, F. A.; Sardon, H. Critical Advances and Future Opportunities in Upcycling Commodity Polymers. *Nature* **2022**, *603*, 803−814.
(29) Schneiderman, D. K.; Hillmyer, M. A. 50th Anniversary Perspective: There Is a Great Future in Sustainable Polymers. *Macromolecules* **2017**, *50*, 3733−3749.
(30) Song, Y.; Ji, X.; Dong, M.; Li, R.; Lin, Y.-N.; Wang, H.; Wooley, K. L. Advancing the Development of Highly-Functionalizable Glucose-Based Polycarbonates by Tuning of the Glass Transition Temperature. *J. Am. Chem. Soc.* **2018**, *140*, 16053−16057.
(31) Brannigan, R. P.; Dove, A. P. Synthesis, Properties and Biomedical Applications of Hydrolytically Degradable Materials Based on Aliphatic Polyesters and Polycarbonates. *Biomater. Sci.* **2017**, *5*, 9−21.
(32) Ajiro, H.; Takahashi, Y.; Akashi, M.; Fujiwara, T. Surface Control of Hydrophilicity and Degradability with Block Copolymers Composed of Lactide and Cyclic Carbonate Bearing Methoxyethoxyl Groups. *Polymer* **2014**, *55*, 3591−3598.
(33) Jiang, X.; Nie, X.; Guo, X.; Song, C.; Chen, J. G. Recent Advances in Carbon Dioxide Hydrogenation to Methanol via Heterogeneous Catalysis. *Chem. Rev.* **2020**, *120*, 7984−8034.
(34) Sun, D.; Sato, S.; Ueda, W.; Primo, A.; Garcia, H.; Corma, A. Production of C4 and C5 Alcohols from Biomass-Derived Materials. *Green Chem.* **2016**, *18*, 2579−2597.
(35) Häußler, M.; Eck, M.; Rothauer, D.; Mecking, S. Closed-Loop Recycling of Polyethylene-Like Materials. *Nature* **2021**, *590*, 423−427.
(36) Dewar, M. J. S.; Grifin, A. C. A Thermodynamic Study of the Role of the Central Group on the Stability of Nematic Liquid Crystals. *J. Am. Chem. Soc.* **1975**, *97*, 6662−6666.
(37) Arora, S.; Fergason, J.; Taylor, T. Molecular Structure and Liquid Crystallinity. Phenylene Bis(alkoxybenzoates). *J. Org. Chem.* **1970**, *35*, 4055−4058.
(38) Dewar, M. J. S.; Goldberg, R. S. The Role of *p*-Phenylene Groups in Nematic Liquid Crystals. *J. Am. Chem. Soc.* **1970**, *92*, 1582−1586.
(39) Lohmeijer, B. G. G.; Pratt, R. C.; Leibfarth, F.; Logan, J. W.; Long, D. A.; Dove, A. P.; Nederber, F.; Choi, J.; Wade, C.; Waymouth, R. M.; Hedrick, J. L. Guanidine and Amidine Organocatalysts for Ring-Opening Polymerization of Cyclic Esters. *Macromolecules* **2006**, *39*, 8574−8583.
(40) Fukushima, K.; Nozaki, K. Organocatalysis: A Paradigm Shift in the Synthesis of Aliphatic Polyesters and Polycarbonates. *Macromolecules* **2020**, *53*, 5018−5022.
(41) Fukushima, K.; Honda, K.; Inoue, Y.; Tanaka, M. Synthesis of Antithrombotic Poly(carbonate-urethane)s through a Sequential Process of Ring-Opening Polymerization and Polyaddition Facilitated by Organocatalysts. *Eur. Polym. J.* **2017**, *95*, 728−736.
(42) Davis, F. J. Liquid-Crystalline Elastomers. *J. Mater. Chem.* **1993**, *3*, 551−562.
(43) Wen, Z.; McBride, M. K.; Zhang, X.; Han, X.; Martinez, A. M.; Shao, R.; Zhu, C.; Visvanathan, R.; Clark, N. A.; Wang, Y.; Yang, K.; Bowman, C. N. Reconfigurable LC Elastomers: Using a Thermally Programmable Monodomain to Access Two-Way Free-Standing Multiple Shape Memory Polymers. *Macromolecules* **2018**, *51*, 5812−5819.
(44) Kato, T. Self-Assembly of Phase-Segregated Liquid Crystals Structures. *Science* **2002**, *295*, 2415−2418.
(45) Young, T. J.; Monclus, M. A.; Burnett, T. L.; Broughton, W. R.; Ogin, S. L.; Smith, P. A. The Use of the PeakForceTM Quantitative Nanomechanical Mapping AFM-Based Method for High-Resolution Young's Modulus Measurement of Polymers. *Meas. Sci. Technol.* **2011**, *22*, No. 125703.
(46) Dokukin, M. E.; Sokolov, I. Quantitative Mapping of the Elastic Modulus of Soft Materials with HarmoniX and PeakForce QNM AFM Modes. *Langmuir* **2012**, *28*, 16060−16071.
(47) Derjaguin, B. V.; Muller, V. M.; Toporov, Y. P. Effect of Contact Deformations on the Adhesion of Particles. *J. Colloid Interface Sci.* **1975**, *53*, 314−326.
(48) Farah, S.; Anderson, D. G.; Langer, R. Physical and Mechanical Properties of PLA, and Their Functions in Widespread Applications − A Comprehensive Review. *Adv. Drug Delivery Rev.* **2016**, *107*, 367−392.
(49) Pêgo, A. P.; Grijpma, D. W.; Feijen, J. Enhanced Mechanical Properties of 1,3-Trimethylene Carbonate Polymers and Networks. *Polymer* **2003**, *44*, 6495−6504.
(50) Montagna, V.; Takahashi, J.; Tsai, M.-Y.; Ota, T.; Zivic, N.; Kawaguchi, S.; Kato, T.; Tanaka, M.; Sardon, H.; Fukushima, K. Methoxy-Functionalized Glycerol-Based Aliphatic Polycarbonate: Organocatalytic Synthesis, Blood Compatibility, and Hydrolytic Property. *ACS Biomater. Sci. Eng.* **2021**, *7*, 472−481.
(51) Fukushima, K.; Jones, G. O.; Horn, H. W.; Rice, J. E.; Kato, T.; Hedrick, J. L. Formation of Bis-Benzoxazole and Bis-Benzimidazole through Organocatalytic Depolymerization of Poly(ethylene terephthalate) and Its Mechanism. *Polym. Chem.* **2020**, *11*, 4904−4913.
(52) Saito, K.; Jehanno, C.; Meabe, L.; Olmedo, J.; Mecerreyes, D.; Fukushima, K.; Sardon, H. From Plastic Waste to Polymer Electrolytes for Batteries through Chemical Upcycling of Polycarbonate. *J. Mater. Chem. A* **2020**, *8*, 13921−13926.
(53) Ishige, R.; Ishii, T.; Tokita, M.; Koga, M.; Kang, S.; Watanabe, J. Well-Ordered Lamellar Microphase-Separated Morphology of an ABA Triblock Copolymer Containing a Main-Chain Liquid Crystalline Polyester as the Middle Segment. *Macromolecules* **2011**, *44*, 4586−4588.

https://doi.org/10.1021/acs.macromol.2c01747
Macromolecules 2022, 55, 10285−10293